



***Facultad
de
Ciencias***

**DISEÑO Y CARACTERIZACIÓN DE UN
ESPECTROPOLARÍMETRO DE IMAGEN**
(Design and characterization of an imaging
spectropolarimeter)

Trabajo de Fin de Grado
para acceder al

GRADO EN FÍSICA

Autor: Andrea Fernández Pérez

Director: José María Saiz Vega

Co-Director: Juan Marcos Sanz Casado

Septiembre-2014

Agradecimientos

Quiero expresar mi agradecimiento:

A Chema y Juanma, por su tiempo, ayuda y consejos,
al equipo de The Zia Lab por la experiencia vivida
y a mi familia y amigos por su apoyo.

INDEX

0. PREFACE	8
0.1. Abstract and key words.....	8

BLOCK I

1. INTRODUCTION	10
1.1. Objectives.....	11
1.2. Work Scheme	11
2. THEORY	13
2.1. Maxwell's Equations.....	14
2.2. Polarized Light	15
2.3. Polarimetry	15
2.3.1. Jones Formalism	15
2.3.2. Mueller-Stokes Formalism	16
2.4. Supercontinuum spectrum generation	18
2.5. Diffraction Grating.....	20
2.5.1. Blaze Grating	21
3. EXPERIMENTAL SETUP	23
3.1. Dual Rotating Compensator Polarimeter	23
3.1.1. Boot protocol and calibration	24
3.2. Supercontinuum Laser.....	25
3.3. Final setup	27
4. RESULTS	31
4.1. Monochromator characterization	31
4.1.1. Spectrometer calibration	31
4.1.2. Wavelength selection	33
4.1.3. Diaphragm aperture	35
4.2. Reproducibility of results	36
4.3. DRCP calibrations at different wavelengths	39
4.1.1. Study of a linear polarizer	40
5. CONCLUSIONS AND FUTURE WORK	42
6. BIBLIOGRAPHY	44

BLOCK II

1. INTRODUCTION	47
2. TASKS	48
2.1. Daily life	48
2.2. Compulsory training courses	48
2.3. Movement of a rotating stage using Matlab Executable (Mex) files	49
3. BIBLIOGRAPHY	51

0. PREFACE

The present final degree project has been carried out at two different Universities and departments. The work done in each place is independent and about different topics. Therefore, this work is divided into two main parts or blocks corresponding to the work realized in each place.

Block I describes the work done at the University of Cantabria, which is the main part of the final degree project. It was developed during the months of February to early June at the Optics Department, under the supervision of Jose María Saiz Vega and Juan Marcos Sanz Casado.

Block II summarizes the part of the work carried out at the University of Brown (Providence, EE.UU). This block is a complement because of the internship program done at the School of Engineering from June 15 to August 8 under the direction of Prof. Rashid Zia.

0.1. Abstract and key words

Resumen

La espectropolarimetría tiene como objetivo el análisis simultáneo del espectro y la polarización de la luz.

El propósito de este proyecto es transformar el polarímetro dinámico de imagen, presente en el laboratorio de óptica del Departamento de Física Aplicada de la Universidad de Cantabria, en un espectropolarímetro de imagen. Se instalará una fuente laser de supercontinuo, desarrollando y caracterizando un monocromador que permita seleccionar, de manera automática, la longitud de onda deseada dentro del espectro visible. Posteriormente, se calibrará el funcionamiento conjunto de todo el sistema. De esta manera, seremos capaces de estudiar la polarización de la luz y de realizar medidas de la matriz de Mueller a diferentes longitudes de onda.

Para lograr este objetivo, el espectro continuo será separado angularmente en las diferentes longitudes de onda mediante una red de difracción situada en una plataforma giratoria. A continuación, se seleccionará una parte del espectro con un diafragma. Finalmente, el polarímetro de imagen, junto con la nueva fuente, será calibrado y puesto a prueba sobre algún elemento óptico.

Palabras clave: espectropolarimetría, polarímetro, matriz de Mueller, vector de Stokes, red de difracción, monocromador, supercontinuo.

Abstract

The simultaneous analysis of the spectrum and state of polarization of light is usually referred to as spectropolarimetry.

The main objective of this project is to transform the imaging dynamic polarimeter located at the optics laboratory of the Departamento de Física Aplicada at Universidad de Cantabria, into an imaging spectropolarimeter. This project aims to implement a new supercontinuum laser source and to develop and characterize a monochromator which will allow selecting the operating wavelength in an automated way. The whole setup will be calibrated in a later stage. Thus, we will be able to study the polarization of light and to perform measurements of the Mueller matrix at different wavelengths, in a wide range of the visible spectrum.

In order to do that, the continuous spectrum will be angularly dispersed by a diffraction grating placed on a rotating platform. Then, a fraction of the spectrum will be selected by means of a diaphragm.

The imaging polarimeter, working with this fully characterized spectral source, will be calibrated and tested on basic optical elements.

Key words: spectropolarimetry, polarimeter, Mueller matrix, Stokes vector, diffraction grating, monochromator, supercontinuum spectrum.

BLOCK I**1. INTRODUCTION**

Spectropolarimetry consists in the simultaneous analysis of the spectrum and state of polarization of light. This analysis is of great interest when we study the interaction of light with a system that both affects its polarization and shows a spectral dependence.

This technique is widely used for many purposes in fields such as astronomy, medicine, biology or chemistry.

When light interacts with matter it may suffer reflection, refraction, absorption, scattering, dispersion or transmission. These processes can affect the state of polarization of the light and have an effect on the polarization of the overall transmittance, reflectance or absorption of the system.

Because the interaction may be spectrally selective, polarimetry combines with spectral analysis to produce spectropolarimetry.

Spectropolarimetry is used, for example, to study the atmosphere and to find biosignatures in exoplanets [1, 2]. This is possible because when light, that comes from a star, is reflected in a planet, it acquires a certain degree of polarization. This process is related to the interaction of light with the planet's atmosphere and, therefore, with its chemical components.

Also, spectropolarimetry is used to study magnetic fields in stars, black holes, active galaxies, etc... [3] since they polarize the light in different ways too.

Other fields where this technique is applied are remote sensing [4], to study fields, tides, or the movement of glaciers; or chemistry, alimentation or quality control, since certain molecules, called chiral molecules, have optical activity (rotate the plane of polarization) [5]. So the analysis with light can be useful to determinate the concentration of certain substances.

Moreover, in the last ten years, these techniques have found applications on the medical field mainly because of their non invasive character. For example, spectropolarimetry can be used to study biological tissues and cells suspensions [6, 7] because the state and degree of polarization of light can give information about the composition or the structure of a tissue.

1.1. Objectives

The main objective of this project is to transform the imaging dynamic polarimeter located at the optics laboratory, into a spectropolarimeter.

The dynamic polarimeter was developed by Juan Marcos Sanz Casado during his doctoral thesis [8]. Recently, the setup has been improved twice, the first time by Cristina Extremiana [9] and the second by Francesco Carmagnola [10], by implementing, respectively, a discrete wavelength source and an imaging system on a monochromatic basis.

In that stage, the polarimeter worked with a He-Ne laser source which only allows single wavelength measurements. The problems derived from the first spectral-source attempt (instability, cooling problems, discrete offer of wavelengths, high power variations among lines) ended with the implementation of a supercontinuum laser as a spectral source.

Then, this project aims to replace the He-Ne source by a supercontinuum laser and to develop and characterize a monochromator which will allow selecting the wavelength from the visible continuum spectrum. This way, we will be able to study the polarization of light and to perform measurements of the Mueller matrix at different wavelengths, in a wide range of the visible spectrum.

In order to do that, the continuous spectrum provided by the new laser source will be angularly separated in the different wavelength by a diffraction grating. Then, a fraction of the spectrum will be selected by means of a diaphragm. The grating will be placed in a rotating platform controlled by a PC so different wavelengths can be selected in an automated way. The spectral width of the transmitted beam will also be expressed as a function of the diaphragm.

The imaging polarimeter, working with this fully characterized spectral source, will be calibrated and tested on samples consisting on optical elements like retarders or polarizers.

1.2. Work scheme

From here, the work is divided into four sections.

Section 2 presents the basic theory and concepts and the theory on electromagnetism and polarimetry necessary to understand and develop the current project.

Section 3 describes the experimental set up used to perform the measurements. In this section the three main parts of the experimental set up are fully detailed: polarimeter, supercontinuum laser source and the monochromator system.

Section 4 shows the main results. In first place, those corresponding to the source characterization and then, the polarimeter test ones.

Finally, section 5 is devoted to summarize the tasks carried out and to indicate future working lines.

2. THEORY

2.1. Maxwell's equations

Maxwell's equations describe the propagation of an optical field in a medium [11]:

$$\begin{aligned}
 \nabla \cdot \mathbf{D} &= \rho \\
 \nabla \times \mathbf{E} &= -\frac{\partial \mathbf{B}}{\partial t} \\
 \nabla \cdot \mathbf{B} &= 0 \\
 \nabla \times \mathbf{H} &= \mathbf{J} + \frac{\partial \mathbf{D}}{\partial t}
 \end{aligned} \tag{2.1}$$

Where \mathbf{E} and \mathbf{H} are the electric and magnetic field, \mathbf{B} is the magnetic induction ($\mathbf{B} = \mu\mathbf{H}$), \mathbf{D} is the electric displacement field, \mathbf{J} is the density of current ($\mathbf{J} = \sigma\mathbf{E}$) and ρ is density of charge.

\mathbf{D} and \mathbf{B} are related to \mathbf{E} and \mathbf{H} by the equations:

$$\mathbf{D} = \varepsilon_0 \mathbf{E} + \mathbf{P} \tag{2.2}$$

$$\mathbf{H} = \frac{\mathbf{B}}{\mu_0} - \mathbf{M} \tag{2.3}$$

Where \mathbf{P} and \mathbf{M} are the electric polarization and the magnetization, ε_0 is the vacuum permittivity and μ_0 is the vacuum permeability.

From Maxwell's equations together with relations (2.2) and (2.3), the wave equations for \mathbf{E} and \mathbf{B} in a linear medium can be obtained:

$$\nabla^2 \mathbf{E} - \varepsilon\mu \frac{\partial^2 \mathbf{E}}{\partial t^2} = 0 \tag{2.4}$$

$$\nabla^2 \mathbf{B} - \varepsilon\mu \frac{\partial^2 \mathbf{B}}{\partial t^2} = 0 \tag{2.5}$$

Where ε is the electrical permittivity and μ is the magnetic permeability and they are related to the speed of light c by the equation:

$$\frac{1}{c^2} = \varepsilon_0 \mu_0 \tag{2.6}$$

2.2. Polarized light

The polarization is postulated as a transverse property of light. When the electric field \mathbf{E} of a light beam oscillates in a fully predictable way, we say that the light is polarized. For instance, if \mathbf{E} is contained in a plane we say that the light is linearly polarized.

Light can be polarized in other ways: circular or elliptical in such a way that light beam can be totally polarized, partially polarized or even fully depolarized.

Electric field can be separated into three components in the three directions of space. For a polarized beam, if an electric field of amplitude A propagates in the z direction with wave number k and angular frequency ω , then the equations of the electric field components are [12]:

$$\begin{aligned} E_x(t) &= A_x \cos(\omega t - kz + \varphi_x) \\ E_y(t) &= A_y \cos(\omega t - kz + \varphi_y) \\ E_z(t) &= 0 \end{aligned} \tag{2.7}$$

In the general case, the projection of the electric field in a plane perpendicular to the direction of propagation is an ellipse, the polarization ellipse (figure 2.1). This ellipse is given by the equation:

$$\frac{E_x^2(t)}{A_x^2} + \frac{E_y^2(t)}{A_y^2} - \frac{2E_x(t)E_y(t)\cos(\varphi)}{A_x A_y} = \sin^2(\varphi) \tag{2.8}$$

Therefore, in the plane $z = 0$:

$$\begin{aligned} E_x(t) &= A_x \cos(\omega t) \\ E_y(t) &= A_y \cos(\omega t + \varphi) \end{aligned} \tag{2.9}$$

Where φ is the phase difference between the two components:

$$\varphi = \varphi_x - \varphi_y \tag{2.10}$$

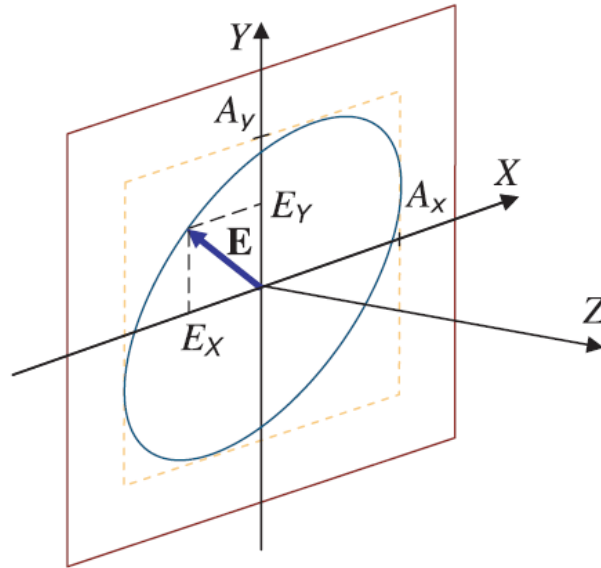


Figure 2.1: polarization ellipse. E_x and E_y are the components of the electric field \mathbf{E} . A_x and A_y are the amplitudes in x and y directions. Z is the direction of propagation.

2.3. Polarimetry

Polarimetry studies the polarization of electromagnetic waves. In order to do that, we need an appropriate formalism to describe the state of polarization of light.

If the light is totally polarized we will use the Jones formalism. However, if the light is partially polarized this formalism will not be enough so that the Mueller-Stokes formalism is needed [13, 14].

2.3.1. Jones formalism:

Totally polarized light can be expressed by means of the Jones calculus developed by R. C. Jones in 1941.

Any polarized state of light can be described by a 2×1 Jones vector and the action of an optical element over the light can be described by a 2×2 Jones matrix. Assuming light propagates in z direction, following Jones formalism, light can be expressed in terms of its electric field \mathbf{E} , with components in the x and y directions. Each one has amplitude and phase so that the Jones vector is:

$$\mathbf{J} = \begin{bmatrix} E_x \\ E_y \end{bmatrix} = \begin{bmatrix} A_x e^{i\phi_x} \\ A_y e^{i\phi_y} \end{bmatrix} \quad (2.11)$$

In order to simplify the expression above we only take into account the phase difference between the two components of the electric field ϕ , as we previously did, so the Jones vector is:

$$\mathbf{J} = \begin{bmatrix} A_x \\ A_y e^{i\phi} \end{bmatrix} \quad (2.12)$$

When a light beam with a Jones vector \mathbf{J} interacts with an optical element the Jones vector at the exit, \mathbf{J}' , is related to \mathbf{J} by the Jones matrix \mathbf{T} of the element.

$$\mathbf{J}' = \mathbf{T}\mathbf{J} = \begin{bmatrix} t_{11} & t_{12} \\ t_{21} & t_{22} \end{bmatrix} \mathbf{J} \quad (2.13)$$

2.3.2. Mueller-Stokes formalism

The Mueller-Stokes formalism describes the polarization state of light and the polarization properties of optical elements. Unlike Jones formalism, which is only valid for totally polarized light, Mueller-Stokes formalism provides a mathematical model useful for unpolarized or partially polarized light.

- Stokes vector:

The Stokes vector \mathbf{S} describes the polarization state of light through four values, called Stokes parameters, defined by G. G. Stokes in 1852.

The Stokes vector can be defined relative to six irradiance measurements I performed with ideal polarizer.

$$\mathbf{S} = \begin{bmatrix} s_0 \\ s_1 \\ s_2 \\ s_3 \end{bmatrix} = \begin{bmatrix} I_0 + I_{90} \\ I_0 - I_{90} \\ I_{45} - I_{135} \\ I_R - I_L \end{bmatrix} \quad (2.14)$$

Where I_0 is the result of the measurement performed with an horizontal linear polarizer, I_{90} with a vertical polarizer, $I_{45,135}$ with a 45° and 135° linear polarizer respectively and $I_{R,L}$ with a right handed and a left handed circular polarizer.

The total intensity of light is: $I = I_0 + I_{90} = s_0$.

From this vector, the following polarization parameters are defined: total flux or intensity I , degree of polarization P , degree of linear polarization P_L and degree of circular polarization P_C .

$$I = s_0 \quad (2.15)$$

$$P = \frac{\sqrt{s_1^2 + s_2^2 + s_3^2}}{s_0} \quad (2.16)$$

$$P_L = \frac{\sqrt{s_1^2 + s_2^2}}{s_0} \quad (2.17)$$

$$P_C = \frac{s_3}{s_0} \quad (2.18)$$

A totally polarized beam has $P = 1$ and a partially polarized beam has $P < 1$.

Another way of write the Stokes vector is:

$$\mathbf{S} = \begin{bmatrix} s_0 \\ s_1 \\ s_2 \\ s_3 \end{bmatrix} = \begin{bmatrix} E_x E_x^* + E_y E_y^* \\ E_x E_x^* - E_y E_y^* \\ E_x E_y^* + E_y E_x^* \\ i(E_x E_y^* - E_y E_x^*) \end{bmatrix} = \begin{bmatrix} A_x^2 + A_y^2 \\ A_x^2 - A_y^2 \\ 2A_x A_y \cos \varphi \\ 2A_x A_y \sin \varphi \end{bmatrix} \quad (2.19)$$

The Stokes vector for a partially polarized beam can be represented as a superposition of a completely polarized Stokes vector \mathbf{S}_P and a completely unpolarized Stokes vector \mathbf{S}_U .

$$\mathbf{S} = \begin{bmatrix} s_0 \\ s_1 \\ s_2 \\ s_3 \end{bmatrix} = \mathbf{S}_P + \mathbf{S}_U = s_0 P \begin{bmatrix} 1 \\ s_1 / s_0 \\ s_2 / s_0 \\ s_3 / s_0 \end{bmatrix} + (1 - P) s_0 \begin{bmatrix} 1 \\ 0 \\ 0 \\ 0 \end{bmatrix} \quad (2.20)$$

- Mueller matrix

The Mueller matrix \mathbf{M} is a 4x4 matrix with real elements that represents the effect of an optical device over the polarization state of the light. It was developed in 1943 by Hans Mueller. This matrix transforms an incident Stokes vector \mathbf{S} into the exiting Stokes vector \mathbf{S}' .

$$\mathbf{S}' = \begin{bmatrix} s'_0 \\ s'_1 \\ s'_2 \\ s'_3 \end{bmatrix} = \mathbf{MS} = \begin{bmatrix} m_{00} & m_{01} & m_{02} & m_{03} \\ m_{10} & m_{11} & m_{12} & m_{13} \\ m_{20} & m_{21} & m_{22} & m_{23} \\ m_{30} & m_{31} & m_{32} & m_{33} \end{bmatrix} \begin{bmatrix} s_0 \\ s_1 \\ s_2 \\ s_3 \end{bmatrix} \quad (2.21)$$

The Mueller matrix fully characterizes a medium for a given wavelength and a geometrical configuration because it contains within its elements all of the polarization properties.

The difficulty of a Mueller matrix analysis is double: first we need to obtain a reliable matrix, and then we have to analyze it in a proper way. For example the Mueller matrix can be decomposed in several matrices each of one represents independent physical actions of the system (diattenuation, retardation and depolarization), though this process is out of the scope of this work.

Any Mueller matrix can be written in the form [15]:

$$\mathbf{M} = m_{00} \begin{bmatrix} 1 & \mathbf{D}^T \\ \mathbf{P} & \mathbf{m} \end{bmatrix} \quad (2.22)$$

Where \mathbf{D}^T is the transposed diattenuation vector, \mathbf{P} is the polarizance vector and \mathbf{m} is a 3x3 matrix related with the optical activity of the medium.

Finally, if the light beam passes through several optical elements the resulting Mueller matrix \mathbf{M}_T is the product of the matrices of each element in reverse order.

$$\mathbf{M}_T = \mathbf{M}_n \mathbf{M}_{n-1} \dots \mathbf{M}_2 \mathbf{M}_1 \quad (2.23)$$

2.4. Supercontinuum spectrum generation

The supercontinuum spectrum is achieved by propagating ultrashort laser pulses through the highly nonlinear optical fiber. Optical fiber becomes a nonlinear medium when high power is propagated through it.

Due to these high pulse-peak powers and high nonlinearity within the fiber, the pulses experience large spectral broadening.

This frequency broadening was first achieved by R. Alfano in 1969 when he propagated picosecond pulses through several materials as calcite and quartz. [16]

A nonlinear medium is a medium where the polarization vector \mathbf{P} does not change linearly with the electric field \mathbf{E} .

In this type of medium, the relation between \mathbf{P} and \mathbf{E} can be expressed as a Taylor series expansion [17]:

$$\mathbf{P} = \epsilon_0 \chi \mathbf{E} + \epsilon_0 \chi^{(2)} \mathbf{E}^2 + \epsilon_0 \chi^{(3)} \mathbf{E}^3 + \dots \quad (2.24)$$

Where the coefficients $\chi^{(n)}$ are the n -th order susceptibilities of the medium.

In nonlinear mediums several effects are produced. They can be classified in two types:

- Elastic effects: there is no energy exchange between the electric field and the material medium. They occur through nonlinear modification of the refractive index of the material. Some of these effects are Four Wave Mixing (FWM), Cross-Phase Modulation (XPM) or Self-Phase Modulation (SPM).

- Inelastic effects: there is energy exchange between the field and the medium. The interaction happens through modification in the material polarizability associated with vibration of the atoms in the lattice. Some of these effects are Stimulated Raman Scattering (SRS) and Stimulated Brillouin Scattering (SBS).

Of course, together with nonlinear effects, there are also linear effects as chromatic dispersion and group velocity dispersion (GVD). Chromatic dispersion is the frequency dependence of the refractive index $n(\omega)$ of the fiber.

GVD is the frequency dependency of the group velocity in a medium which causes pulses to enlarge in time.

So, when the short pulses propagate through the fiber, linear and nonlinear effects affect to the shape and spectrum of the pulses.

As optical fibers are principally made of silica, which has an inversion center, the second order nonlinear effects are neglected as the second order susceptibilities is

zero. As a result, the nonlinear effects in optical fibers originate from the third order susceptibility, which is responsible for phenomena such as third-harmonic generation, four-wave mixing and nonlinear refraction.

On the other hand, higher order nonlinear effects can be neglected because they are very small.

2.5. Diffraction grating

A diffraction grating is an optical element with a periodic pattern (grooves or slits) which diffract the light incident on it. There are reflective and transmission gratings.

Light incident on a grating (figure 2.2) suffers diffraction in each element of the grating. So, in principle, a beam of white light incident on a grating will be spread in all direction. Due to the periodicity of the diffracting element, all diffracted waves are similar and phase-shifted, being the shift related to the period of the grating and the direction of the output beam.

In most directions light suffers destructive interference but in some directions the slits are multiples of 2π and the interference is constructive. These directions are called diffraction orders.

The equation that governs the direction of the diffractive rays, for the case depicted in figure 2.2, is [18]:

$$\sin \theta_m = -\sin \theta_i + m \frac{\lambda}{d} \quad (2.25)$$

Where θ_i is the incident angle, θ_m is the diffracted angle, m is the diffraction order ($m = 0, 1, 2 \dots$), λ is the wavelength and d is the period of the grating.

The resolving power R of a diffraction grating is a measure of its ability to separate adjacent spectral lines of average wavelength λ and is given by the equation:

$$R = \frac{\lambda}{\Delta\lambda} = mN = mkW \quad (2.26)$$

Where m is the diffraction order, k is the groove density, N is the number of grooves illuminated, W is the illuminated width, λ is the wavelength and $\Delta\lambda$ is the limit of resolution or smallest resolvable wavelength difference.

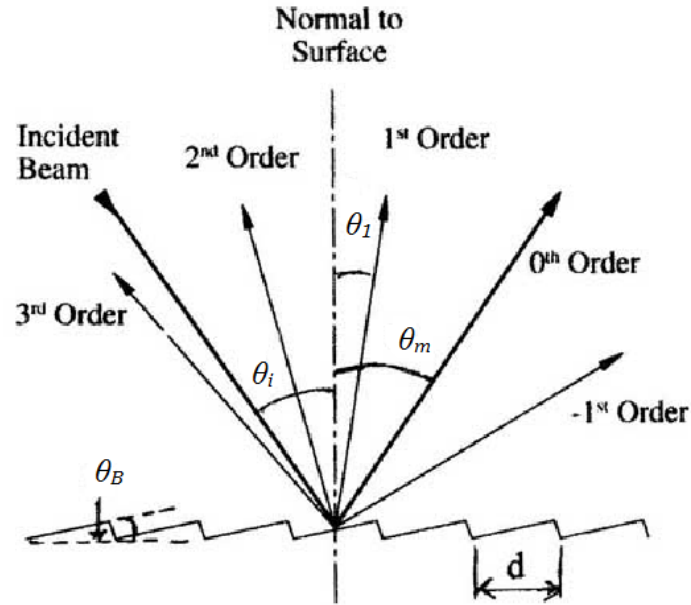


Figure 2.2: reflective diffraction blaze grating. The light beam has an incident angle θ_i and a diffraction angle θ_m . Blaze angle θ_B is shown.

2.5.1. Blaze grating:

There is a special type of grating called blaze grating. It is characterized by having a saw-tooth surface with a blaze angle θ_B and it is constructed in order to concentrate the maximum efficiency for a combination of θ_i and θ_m , for a given period and order (usually the 1st order) that correspond to a certain wavelength called blaze wavelength λ_B .

There is a particular configuration called the Littrow configuration (figure 2.3) in which $\theta_i = \theta_m = \theta_B$ for a certain order m .

In this configuration the incident ray of light is perpendicular to the groove surface, something that helps to understand the efficiency mechanism of Blaze gratings.

In Littrow configuration, from equation (2.25) we can obtain the blaze wavelength for a given period d and blaze angle.

$$2 \sin \theta_B = m \frac{\lambda_B}{d} \quad (2.27)$$

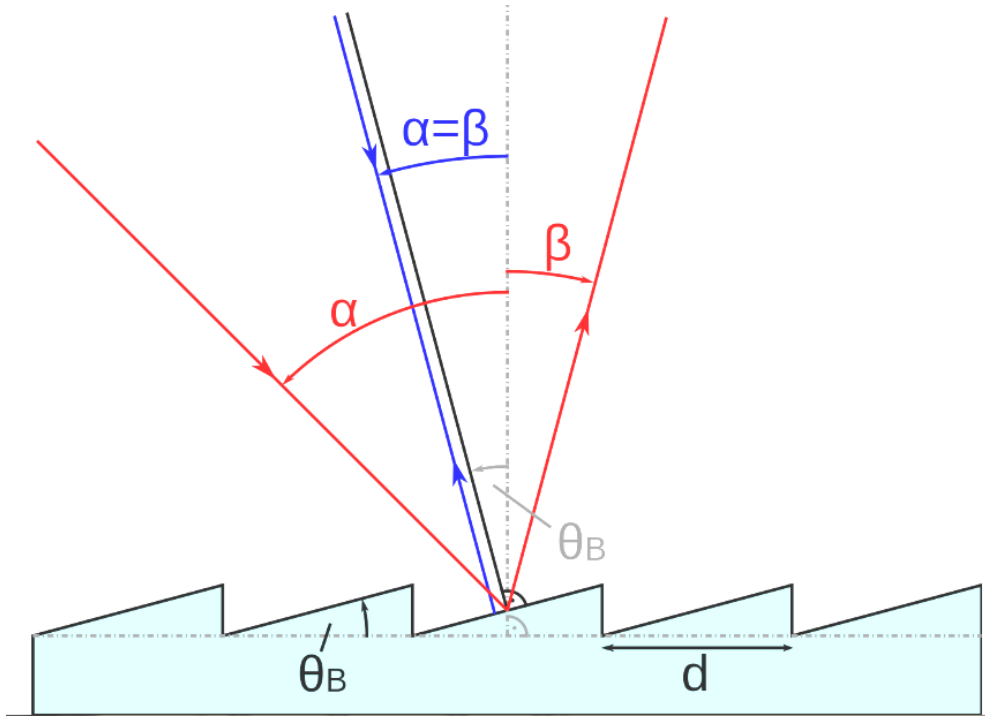


Figure 2.3: blaze grating in Littrow configuration. θ_i is the incident angle, θ_m is the diffraction angle, θ_B is the blaze angle and d is the period of the grating.

The diffraction grating used in this project is a 12.7x12.7x6 mm blaze grating made by Thorlabs [19]. Its groove density is $k = 1800$ g/mm ($d = 555.55$ nm) and it has a blaze wavelength of $\lambda_B = 500$ nm and a Blaze angle $\theta_B = 26^\circ 44'$. The grating has a dispersion of 0.5 nm/mrad and a damage threshold of 40 W/cm². It is going to be used in order to expand the continuum and separate the different wavelengths.

3. EXPERIMENTAL SETUP

3.1. Dual Rotating Compensator Polarimeter (DRCP)

The main instrument used is the Dynamic Rotating Compensator Polarimeter (DRCP) (figure 3.1) located in the Optics laboratory at the Universidad de Cantabria. This device was developed by Juan Marcos Sanz Casado. Moreover, the device has been recently improved by Francesco Carmagnola who added a CCD detector and wrote software in OCTAVE code to obtain a fully Mueller imaging system.

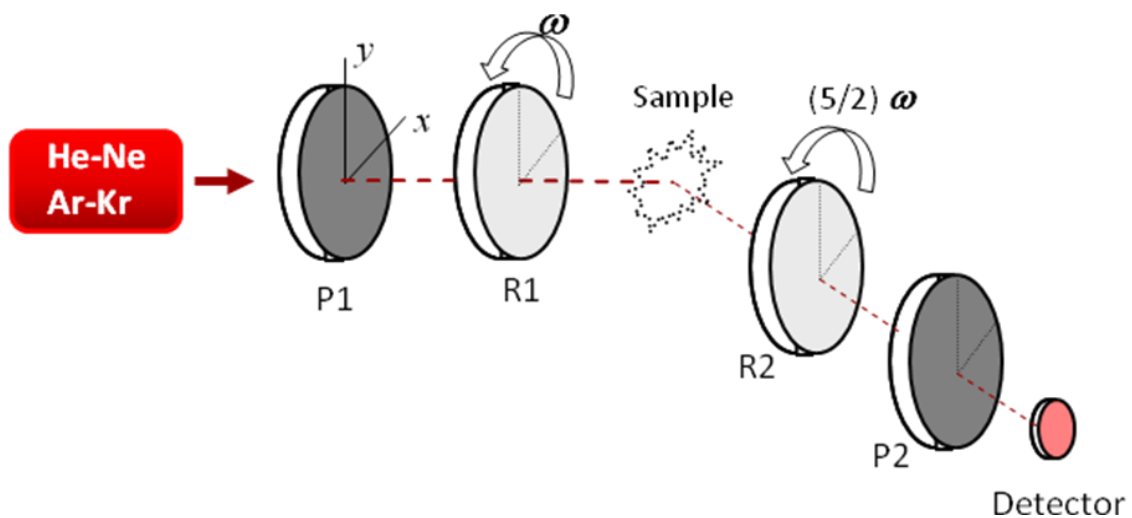


Figure 3.1: Dual Rotating Compensator Polarimeter [8].

The polarimeter consists of an He-Ne laser source, to be replaced by a supercontinuum laser as part of this project; a polarization state generator (PSG) composed of a polarizer and a rotating quarter-wave plate; a polarization state analyzer (PSA) composed of an analyzer and a rotating quarter-wave plate; and a detector. The detector has been recently improved and replaced by a CCD camera so that now we are able to obtain a full image of the illuminated area of the sample.

Right after the laser source a long focal-length lens is placed in order to control the spot size and to focus light on the sample. Between the PSG and the PSA there is a sample holder where the sample we want to study is placed. The intersection point formed by the alignment axis system and the detection system axis correspond to the center of the observed area of the sample. If the sample is going to be rotated as a part of the experiment the rotation axis must also contain such intersecting point.

Both quarter-wave plates rotate synchronously with a speed ratio of 5:2 so we can complete a full Fourier cycle made of 200 measurements of the intensity. The data obtained from the cycle is saved in raw format and it is used to calculate, by means of a Fourier analysis [20], the Mueller Matrix (MM) of the sample placed between the PSG and the PSA.

The PSA together with the detector are set in an arm which can rotate so that the MM of a sample can be measured in different configurations such as transmission, reflectance or scattering.

This movement is performed by a motor controlled with software. The two wave plates both are moved by stepper motors and when the full cycle is finished they return to its original position.

3.1.1. Boot protocol and calibration:

When we want to perform a measure of the Mueller matrix it is very important to follow a boot protocol to guarantee the correct work of the experimental set up.

Moreover, we need to calibrate the polarimeter every time we modify some of the optical elements.

In this section it will be described in detail how to calibrate the polarimeter. This is a very important point of the work as it is essential to do a correct calibration in order to obtain good results in a measure.

The calibration involves expanding the beam of the laser and doing a full cycle of measures without placing a sample between the PSA and the PSG.

After turning on the full experimental setup it is time to calibrate the system.

With both arms of the polarimeter aligned, we should start with the PSA, this is, the farthest elements, as seen from the source.

With the lights off we should cover the camera/detector with a white foil in order to avoid CCD sensor's damage. Next, we should remove both wave plates and search for the maximum contrast with the laser. After this, we cross the analyzer (PSA) and we look for the minimum intensity.

The next step is to place the PSA wave plate and, as we just did with the polarizer, we look for the minimum, by rotating it until the neutral axis of the wave plate is aligned with the PSA polarizer. At this point we should not forget to turn on the wave plate motor. We repeat the process for the PSG wave plate.

We move on now to the PSA polarizer and, the one away from the laser and we rotate this polarizer 90 degrees clockwise and 22.5 degrees anticlockwise. This 22.5° is not a random angle but it is known to be adequate to minimize the error in the measured cycle.

After this procedure, we are ready to do a measurement cycle. As there is no sample, we measure the intensity transmitted by the air. The Mueller matrix of the air, \mathbf{M}_a , is approximated by the vacuum Mueller matrix \mathbf{M}_v : the 4x4 unit matrix.

$$\mathbf{M}_v = \begin{bmatrix} 1 & 0 & 0 & 0 \\ 0 & 1 & 0 & 0 \\ 0 & 0 & 1 & 0 \\ 0 & 0 & 0 & 1 \end{bmatrix} \quad (3.1)$$

3.2. Supercontinuum laser

In supercontinuum generation, the light from a laser (monochromatic) is transformed in light with a very broad spectrum but keeping a high spatial coherence characteristic of lasers.

This broad spectrum is achieved by propagating ultrashort laser pulses through a highly non linear medium, like optical fibers, as we already explained in section 2.4.

The source we use in this project is a FemtoPower 1060 Supercontinuum Laser Source by Fianium [21]. It provides an average spectral power of 1mW/nm and it generates a continuous spectrum from 450 to 2400 nm approximately. The spectral power density is not constant with the wavelength. For example, it reaches a peak of nearly 12 mW/nm in the infrared region. The frequency of the pulses is 20 MHz.

The laser can be controlled manually by means of the controls on the rear panel or through computer software. The output power can vary by changing an intrinsic parameter of the cavity, Q , from $Q = 0$ to 4000.

In the rear panel (figure 3.2) there are both a USB connector and a SMA connector in order to control the laser from a computer and to monitor the pulses produced by the master source. Also, there is a power connector to supply energy to the laser and an interlock connector for safety purposes.

The master source is switched on by pressing a button but the laser emission does not begin until the amplifier is enabled with the key switch.

Every time the laser is connected it takes around ten minutes until it reaches the optimal temperature to work.

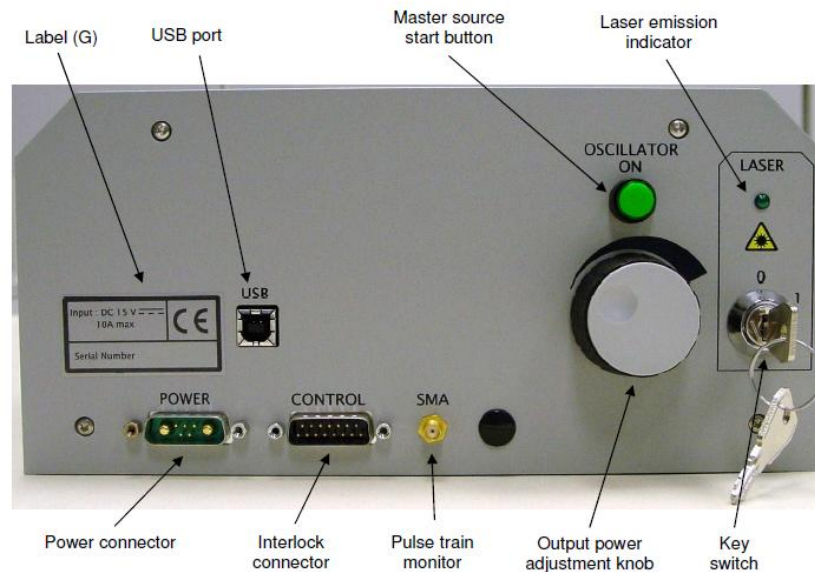


Figure 3.2: supercontinuum laser rear panel [21].

The supercontinuum laser consists of three main parts (figure 3.3): a passively mode-locked low power fiber laser (master source), a high power cladding pumped fiber amplifier and a high nonlinearity fiber.

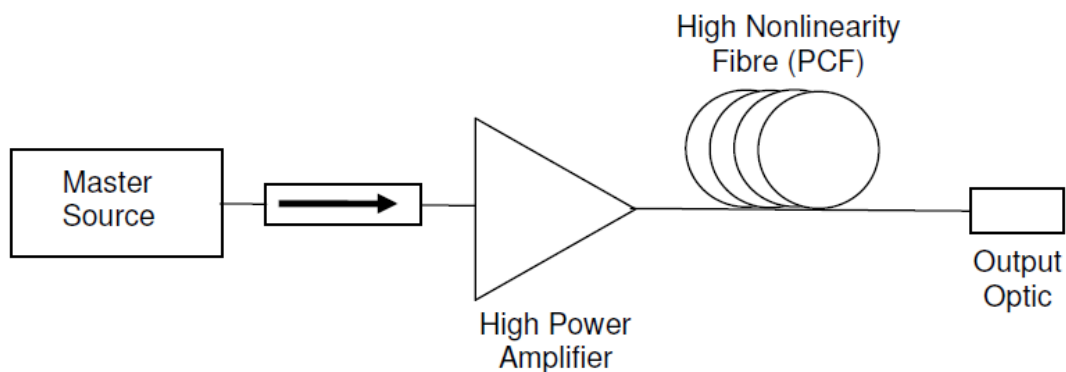


Figure 3.3: diagram of the supercontinuum laser [21]. The three main parts are the master source, the amplifier and the high nonlinearity fiber where the supercontinuum spectrum is achieved.

- *Master source*: the master source is a passively mode locked fiber laser.

Fiber lasers are lasers in which its gain medium, instead of being a semiconductor, is a doped fiber. In this case the fiber is doped with Yb. These type of lasers present quite interesting qualities such as a high gain efficiency that makes them possible to operate with low pump power.

Another important characteristic is that the gain bandwidth of the doping element (Yb) is large which allows the generation of ultra short pulses.

With regard to the operating mode, mode locking [22] is a technique to obtain ultra short pulses in lasers (picoseconds or femtoseconds pulses) introducing a fixed phase between the longitudinal modes of the laser's cavity. There are two types of mode locking: active and passive. In active mode locking the laser resonator contains an active element or optical modulator whereas in passive mode locking a nonlinear passive element or saturable absorber is place inside the resonator cavity. Besides this, passive mode locking allows the generation of shorter pulses (femtosecond pulses).

The saturable absorber is a material with a degree of absorption which is decreases at high optical intensities. It modulates the resonator loses.

- *Power amplifier*: the high power fiber amplifier is based on a doble-clad Yb-dopped fiber, pumped by a high power diode. The power is controller manually by turning the knob in the panel or with the computer.

- *Supercontinuum generator*: the supercontinuum generator consists of a length of highly-nonlinear optical fiber, with dispersion and length tailored to optimize the broadening. In this part is where the broad spectrum is achieved.

3.3. Final setup

In order to select a wavelength to perform the measurement of the Mueller matrix it is necessary to develop a monochromator since the laser source provides a continuum spectrum.

The monochromator (figure 3.4) is composed by a diffraction grating (section 2.5.1), that separates the continuum spectrum, and a diaphragm of variable aperture to select the wavelength.

The grating is placed in a rotating stage made by Thorlabs [23]. This stage can rotate 360° either clockwise or anticlockwise and is controlled either manually with a controller unit or with software from the computer. The grating is placed so that its center is aligned with the rotation axis of the stage, with the laser hitting this same point.

In addition, the stage is placed on another set of platforms which allows us to modify the height and the angles in the horizontal and vertical direction.

The manual movement of the stage is carried through a controller unit (TDC001 DC Servo Motor Drive [24]) which allows rotating the stage a certain angle in a continuous mode or step by step, fixing the step value with the computer.

The software provides information about the position and allows a more accurate control introducing the value of the position you want (in degrees) directly in the display. [The display shows the position of the stage with an accuracy of 4 decimals]. Moreover, we can program a series of movements.

Also, it allows changing the value of the step, the movement mode (continuous or step by step) and the value of the speed rotation.

The laser illuminates the diffraction grating with an incident angle of $\theta_i = 31,4^\circ$ so that the continuous spectrum is expanded, i.e. it is separated by allowing us to select a quasi-monochromatic range. Roughly speaking, the continuous spectrum is separated in the different colors. After the grating, located at 40 cm, it is placed a diaphragm of variable aperture which select the wavelength interval. This illuminating setup is aligned with the rest of the polarimeter; therefore, the light follows the same path as it did with the He-Ne laser source used before.

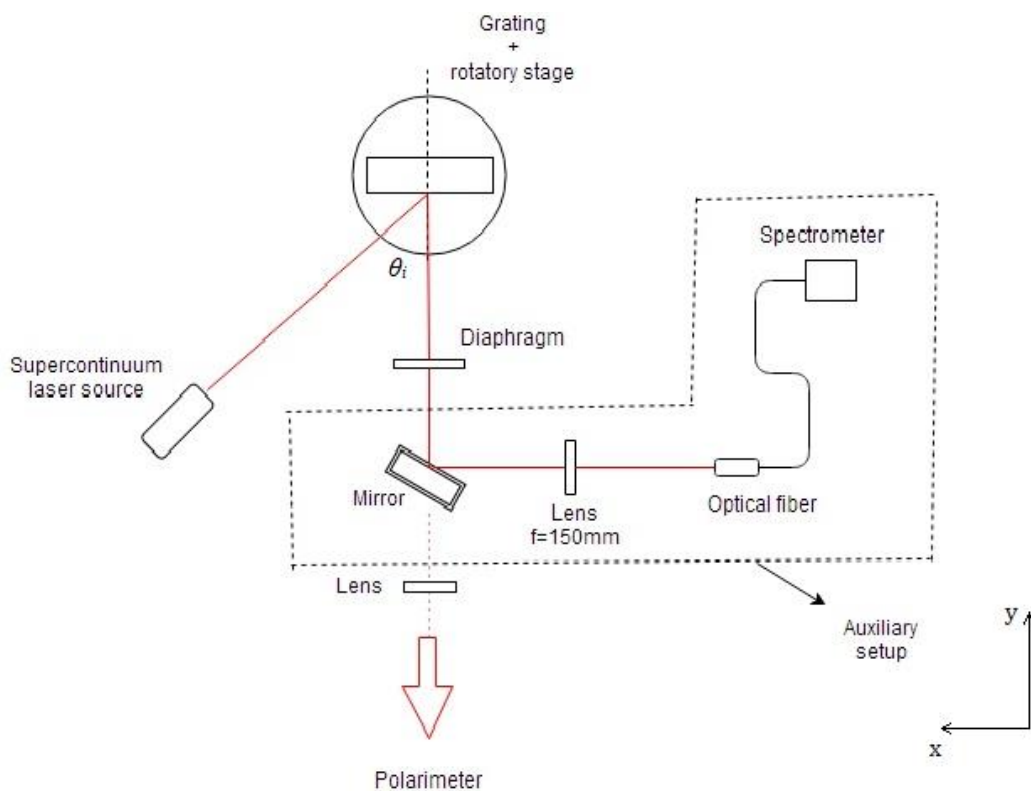


Figure 3.4: monochromator setup (top view). After the monochromator characterization the auxiliary setup is removed so the light passes through the polarimeter.

In order to control the reflected beam in the diffraction grating, i.e. the zero order, a mirror reflects it downwards to a metallic plate located in the table. (It is very important to absorb this beam because it is very energetic in the infrared region and it could burn cables, furniture or clothes placed in its way).

All elements that form the monochromator must be perfectly aligned with the rest of the elements of the polarimeter in order to allow the portion of spectrum selected by the diaphragm to travel through to travel through the whole polarimeter and to reach the detector finally.

Not only is this a non-trivial step, but it is a very important one, because it is necessary to follow a series of instructions in order to be sure that the light will follow the correct path.

First of all, every element of the experimental setup must be at the same height. We take as a reference the elements from the PSG and the PSA since they are already aligned from the previous setup.

Therefore, we must assure that each new element added to the setup (laser source, grating, diaphragm...) are at the same height.

Then all the elements, except for the source, are placed along the same line. This line is defined by the elements of the polarimeter and is parallel to the plane of the table.

In conclusion, the beam of light must follow the straight line formed by four main points: the incident point in the surface of the grating, the hole in the diaphragm, the sample and the detector (figure 3.5). This can be achieved by moving the different elements in the x direction (In the plane xy or plane of the table).

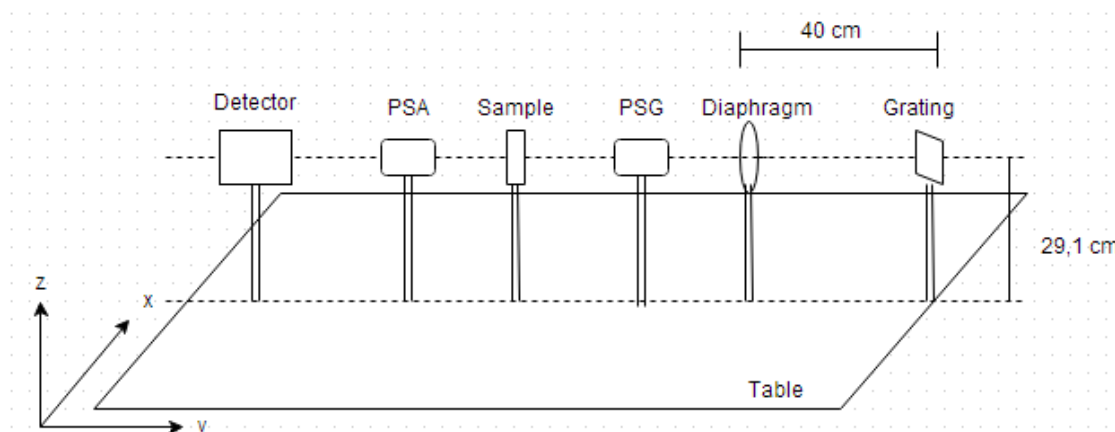


Figure 3.5: diagram of the experimental setup.

Concerning the diffraction grating, its surface normal must be parallel to the plane of the table. Otherwise, the diffracted beams would deviate from its path. This can be achieved by moving the platform which allows changing the inclination of the grating.

The final check of the alignment has been made using as a reference a point in the wall (distant > 5 m) used to align the original He-Ne laser.

Finally, an important aspect to consider is that the rotating stage can be rotated in both directions but the last movement must be always clockwise in order to keep the grating correctly aligned with the rest of the setup.

4. RESULTS

4.1. *Monochromator characterization*

In order to build a monochromator that may be useful in future measurements, an essential step is to fully characterize it. This means to study the wavelength selection for different diaphragm apertures and positions of the diffraction grating. Also, we study the reproducibility of the measures, this is, once we have the curve of selected wavelength as a function of the position/angle of the rotating stage, we do several trials moving the stage to a position and checking if the selected wavelength is the same given by the fitting.

In order to do that, we assemble an auxiliary setup (figure 3.4) in which a mirror diverts the light beam selected by the diaphragm. This beam is focused onto an optical fiber by a biconvex lens of focal 150 mm. The spectrum collected by the fiber is measured by a spectrometer.

4.1.1. *Spectrometer calibration*

In order to control the wavelength selected by the monochromator implemented after the supercontinuum laser, we are going to use a spectrometer. This device will tell us the interval of wavelengths we are selecting from the continuum spectrum.

But, first of all, we need to study the response of the device. This will allow us to know the resolution with which we can measure the wavelength.

We are going to use the spectrometer USB2000 [24], from *Ocean Optics, Inc.* (The spectrometer is powered by a computer through an USB). An optical fiber is attached to the device in order to collect the light from a source. The program reads the counts at several wavelengths and saves this information in a text file which can be imported to a plotting program in order to represent the spectrum graphically.

This small spectrometer is a closed box with an USB port for the power supply and data exchange, and a coupling for the input the optical fiber (See figure 4.1). The light coming from the source is collected by the optical fiber and goes into the spectrometer through the SMA connector (1). Then, there is a slit with a rectangular aperture (2), which regulates the amount of light that enters and controls the spectral resolution. Finally, a filter (3) is found restricts optical radiation to pre-determined wavelength regions.

Inside the device, the light encounters a collimating mirror (4) which focuses the light towards a diffraction grating (5). This grating diffracts the light and guides it to a second mirror (6) which focuses the light onto the detector (8).

This detector, depending on the spectrometer configuration, is a CCD detector or a L2 Detector Collection Lens (9). The last one is used when there is a low light level.

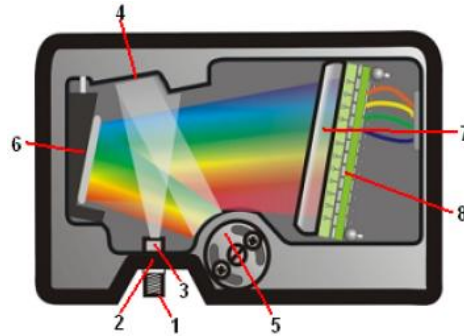


Figure 4.1: spectrometer USB2000 [25]. (1): SMA connector; (2): slit; (3): filter; (4): collimating mirror; (5): diffraction grating; (6): mirror; (7 y (8): detector.

In order to know the resolution achieved by the spectrometer we measured the spectrum of an He-Ne laser since it is formed by a single well-known wavelength of $\lambda_{\text{He-Ne}} = 6328 \text{ \AA}$. First of all, we measure the spectrum of the backlight, with the laser off. Then, we measure the spectrum with the laser on. The software allow us to measure the counts at each wavelength in a fixed range, adjusting the integration time in order to have enough signal but not to saturate the detector.

The backlight spectrum has been subtracted to the measure done with the laser on in order to obtain the spectrum of the laser. The result is presented in figure 4.2.

In the spectrum is observed the peak corresponding to the emission of the laser. Its maximum is at a wavelength $\lambda_{\text{exp}} = 6330 \text{ \AA}$ with a Full Width at Half Maximum of $\text{FWHM} = 1,5 \text{ nm} = 15 \text{ \AA}$.

Comparing the theoretical value and the experimental result, we find a difference of 0,2 nm and a width of 1,5 nm. These will be the precision and resolution values with which we will characterize our instrument, more then enough for our purposes.

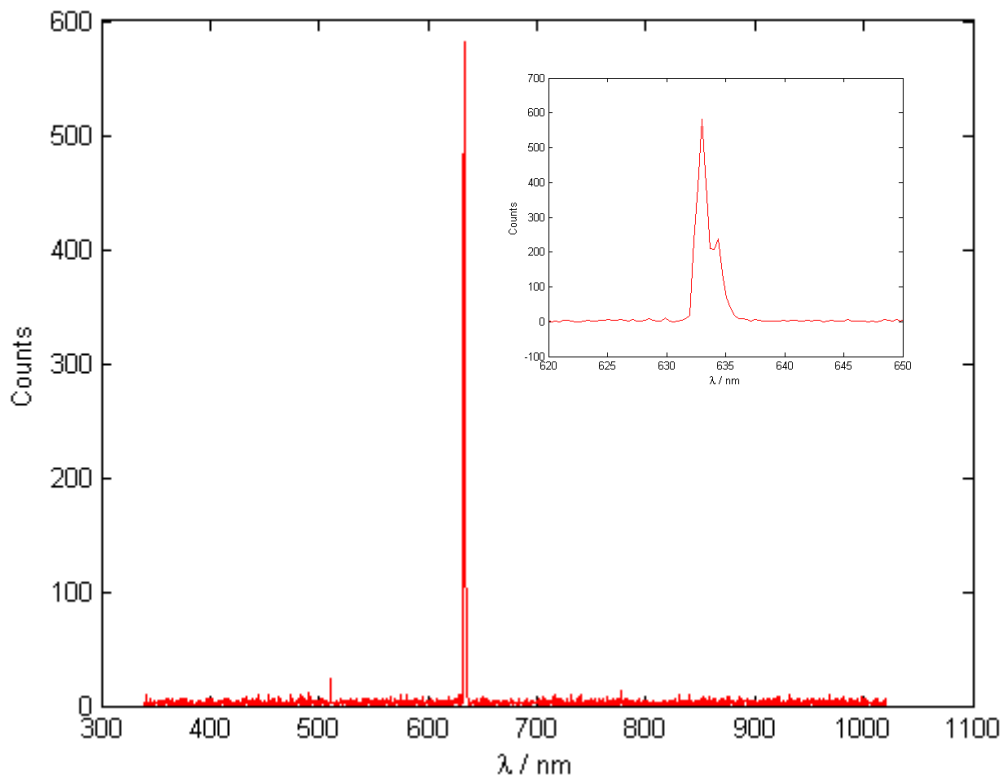


Figure 4.2: He-Ne laser spectrum. $\lambda_{exp} = 6330 \text{ \AA}$, $FWHM = 15 \text{ \AA}$.

4.1.2. Wavelength selection

First of all we achieve the wavelength selection by rotating the grating step by step so that a part of the diffracted light goes through a small diaphragm. This process is characterized by knowing in what angle we must place the grating to obtain a certain wavelength.

As the power given by the laser source is not constant in the entire spectrum, sometimes we have too much light in certain regions of the visible spectrum and the spectrometer is saturated, while in other wavelengths the intensity is so small that the measurement is not possible. Therefore, in order to solve this problem as far as possible, for doing the monochromator characterization, the laser will work at low to intermediate powers. At these powers, the blue region is barely achieved but if we worked at higher powers we would have too much light in other regions.

Working at such high powers is not recommendable because of the heating problems, like the damage caused in the grating, among others.

Figure 4.3 shows four measurements made in different days by moving the stage in 0.5° steps. The angle α corresponds to the position of the stage (not the incident angle) and λ is the maximum wavelength measured with the spectrometer.

Experimental data can be approximated by a straight line: $\lambda = m_1\alpha + b_1$. The fitting results are shown in table 4.1.

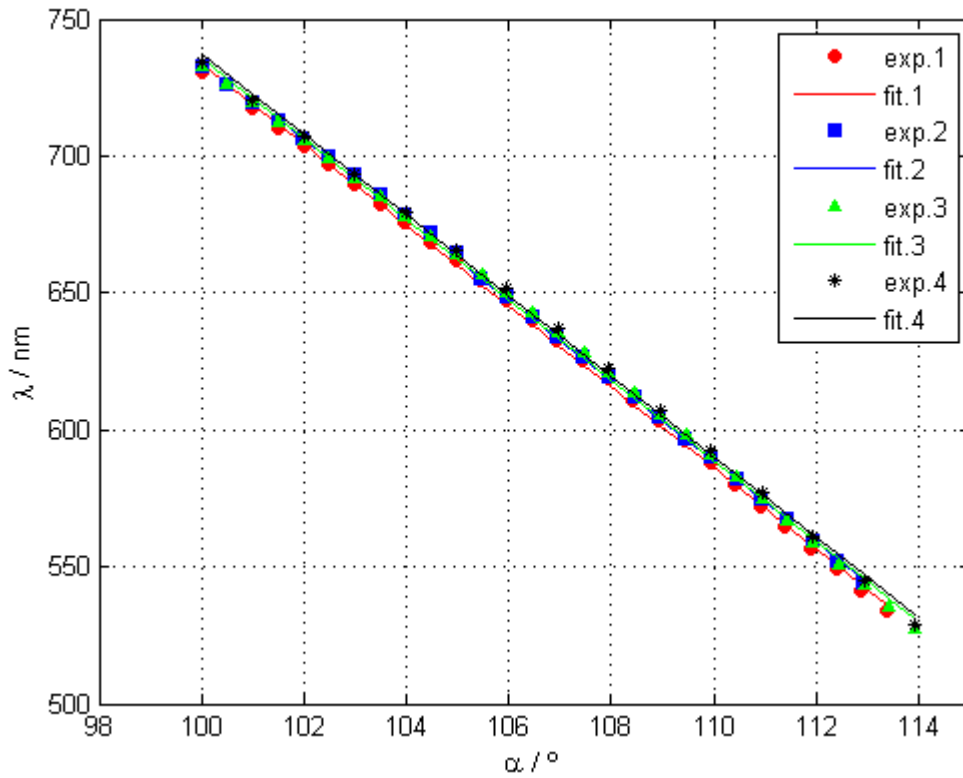


Figure 4.3: wavelength λ as a function of the position of the stage α for four different measurements. The different markers show the experimental points measured. The continuous lines show the best fitting to a straight line.

	1	2	3	4	Mean
$m_1 / \text{nm}/^\circ$	$-14,76 \pm 0,08$	$-14,68 \pm 0,06$	$-14,72 \pm 0,08$	$-14,67 \pm ,11$	$14,71 \pm 0,02$
b_1 / nm	2210 ± 8	2204 ± 6	2208 ± 9	2204 ± 13	2206 ± 2
R	0,99967	0,9998	0,99956	0,99957	

Table 4.1: fitting parameters. m_1 is the slope, b_1 is the intercept and R is the lineal correlation index.

So, from figure 4.3 and table 4.1, we can see that the experimental points fit almost perfect to a straight line of slope $\langle m_1 \rangle = (14,71 \pm 0,02) \text{ nm}/^\circ$.

$$y = -14,71x + 2206 \quad (4.1)$$

This fitting will be used to know the wavelength at a certain position of the grating.

These set of measurements has been done by returning the stage to the initial or zero position manually. This implies a little initial error so it is very hard to place the stage always in the exactly same initial position. However, we see that the fitting are very similar for the three sets of values, therefore, returning the stage to zero manually does not introduce important errors.

It is worth to emphasize that this result is an approximation since the error in the wavelength at a certain angle α may change depending on the accuracy with which the stage is placed at zero initially.

4.1.3. Diaphragm aperture

To complete the monochromator characterization we measure the full width at half maximum (FWHM) of the spectrum selected by the diaphragm with different apertures.

The aperture ϕ varies from 1 mm to 3 mm in steps of 0,2 mm and the laser works at a power of $Q = 700$. Figure 4.3 shows the variation of the FWHM when the aperture increases. The measures have been done at a wavelength of $\lambda = 519,1 \text{ nm}$.

As it was expected the FWHM increases linearly with the size of the aperture (figure 4.4). At first sight, it can be thought that the straight line must pass through the origin (0, 0). However, this is not true since the smallest FWHM, this is, the intercept in figure 4.4 is given by the smallest resolvable wavelength difference $(\Delta\lambda)_{min}$ (equation 2.31).

From this equation we calculate $(\Delta\lambda)_{min}$ [$W_g \approx 1.5 \text{ mm}$ at 530 nm , $m = 1$, $\lambda = 519,1 \text{ nm}$ and $k = 1800 \text{ g/mm}$].

$$R = 2700 \rightarrow (\Delta\lambda)_{min} \approx 0,2 \text{ nm}$$

Comparing the result above with the intercept to the figure, $b_2 = (0,4 \pm 0,1) \text{ nm}$ we see that both are coherent although the results are slightly different. This can be because theoretical calculation is an approximation since we don't really know the

value of the beam diameter at a certain power and wavelength so the number of illuminated grooves may be smaller and so the resolution power R .

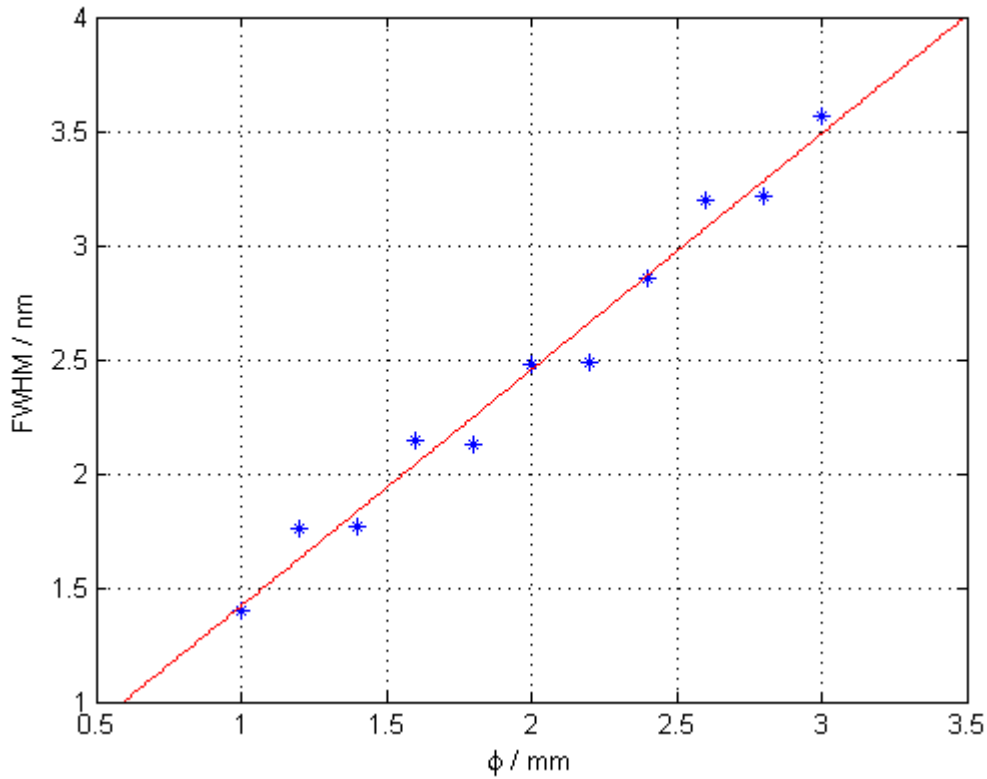


Figure 4.4: full width at half maximum (FWHM) as a function of the diaphragm aperture ϕ . $m_2 = (1,03 \pm 0,05)$, $b_2 = (0,4 \pm 0,1)nm$.

Another interesting aspect that attracts attention from figure above is that the spectral width increases in steps and therefore making the experimental points to appear in couples.

This effect is due to the resolution of the spectrometer that can be assessed to be:

$$\frac{(3,6-1,4)nm}{6} = \frac{2,2}{6} = 0,37 \text{ nm}$$

Therefore, we can't see a variation in the FWHM smaller than this resolution. Despite this fact, it is still appreciable the linear behavior of the figure 4.4.

4.2. Reproducibility of results

In order to perform the alignment of the laser and the monochromator with the rest of the setup (sample + detection area), it was necessary to change the inclination of the diffraction grating and not only its height.

Then, we decided to repeat the measurements done in section 4.2.1. We found that the slope of the straight line in figure 4.3 changed, though only slightly. In figure 4.5 and table 4.2 we can see the final result.

We have made three different measures of the wavelength as a function of the stage position, varying the position of the stage one degree per step. As we did before, the data has been adjusted to a straight line.

So, the final fitting is given by the expression:

$$y = -14,89x + 2194 \quad (4.2)$$

Finally, we decided to check the accuracy of the wavelength selection system that we have characterized. To do that, we took several measurements different positions of the stage and compare the results with the fitting given by the equation (4.2).

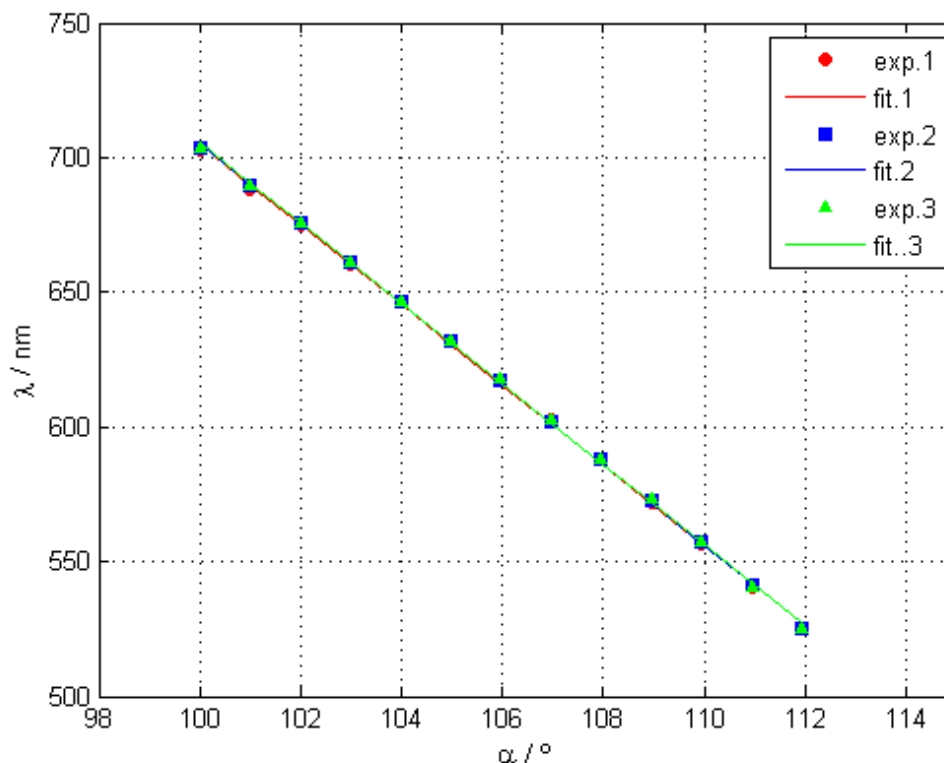


Figure 4.5: wavelength λ as a function of the position α of the stage α for three different measurements after completing the alignment. The different markers show the experimental points measured. The continuous lines show the best fitting to a straight line.

	1	2	3	Mean
$m_1 / \text{nm}/^\circ$	$-14,91 \pm 0,09$	$-14,9 \pm 0,1$	$-14,87 \pm 0,1$	$14,89 \pm 0,01$
b_1 / nm	2196 ± 9	2196 ± 11	2191 ± 10	2194 ± 2
R	0,99975	0,99981	0,99976	

Table 4.2: fitting parameters. m_1 is the slope, b_1 is the intercept and R is the lineal correlation index.

Figure 4.6 shows the straight line obtained from the fitting in table 4.2. This line will tell us what wavelength we are measuring when the stage is placed at a certain angle α .

This figure also shows seven experimental points, in blue. The differences between experimental points and the fitting are shown in table 4.3.

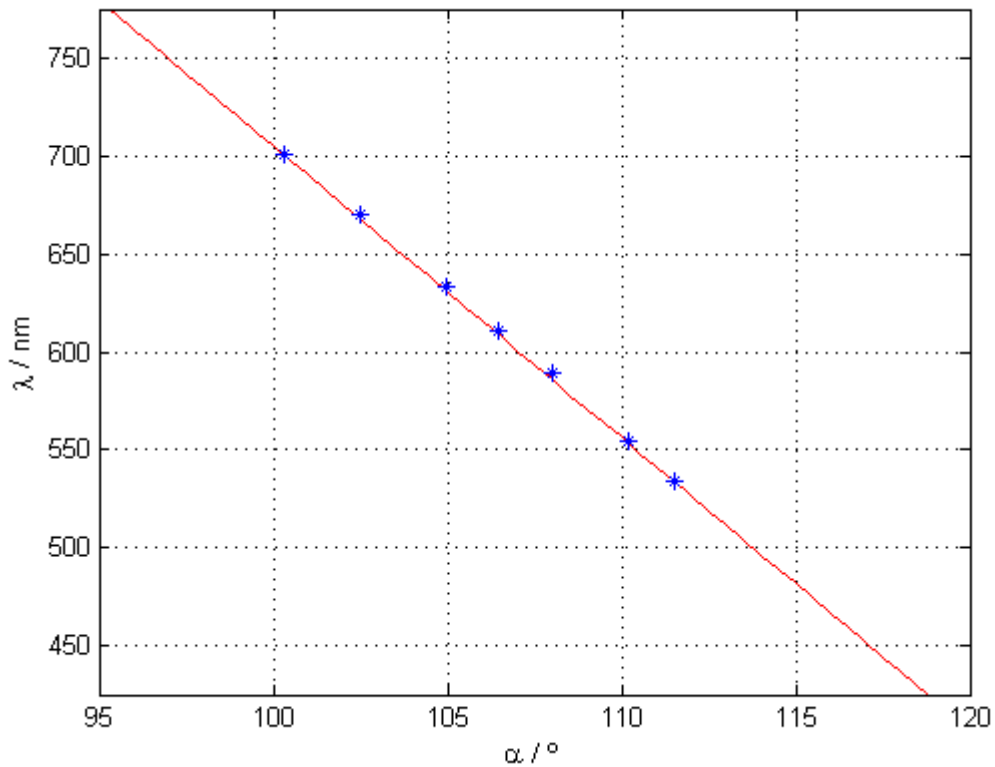


Figure 4.6: final fitting that shows the selected wavelength λ at a certain position of the stage α . The markers show some experimental points. The continuous line is obtained from the measures in figure 4.5

$\alpha / ^\circ$	$\lambda_{exp} / \text{nm}$	$\lambda_{fit} / \text{nm}$	$ \Delta\lambda / \text{nm}$
100,3	700,66	700,54	0,12
102,5	669,94	668,14	1,8
105	632,99	631,02	1,97
106,5	610,51	609,73	0,78
108	588,89	586,14	2,75
110,2	554,75	552,43	2,32
111,5	533,80	534,19	0,39

Table 4.3: position of the stage (α), selected wavelength predicted by the fitting (λ_{fit}), experimental wavelength measured (λ_{exp}) and difference between both of them.

From table 4.3 we see that the differences are less than 3 nanometers, being the average deviation smaller than 2 nm. This is an acceptable error.

4.3. DRCP calibration at different wavelengths

Finally, in order to check that the new source implemented works fine in the DRCP, we have performed some calibration cycles at different wavelengths and we have obtained their Mueller matrices. Ideally, the calibration matrix has to be the identity matrix (equation 3.1).

The measurements have been done with a diaphragm aperture of approx. 1 mm for six positions of the stage at 104, 106, 108, 110, 112 and 114 $^\circ$, which correspond, according to figure 4.6, with the central wavelengths: $\lambda_1 = 645 \text{ nm}$, $\lambda_2 = 616 \text{ nm}$, $\lambda_3 = 586 \text{ nm}$, $\lambda_4 = 556 \text{ nm}$, $\lambda_5 = 526 \text{ nm}$ and $\lambda_6 = 497 \text{ nm}$. Intensity patterns are shown in figure 4.7.

Figure 4.8 shows some examples of the calibration Mueller matrices at $\lambda_2 = 616 \text{ nm}$ and $\lambda_4 = 556 \text{ nm}$. We have achieved pretty good calibration matrices, but the fact that we didn't get a homogeneous intensity of the beam makes harder to get a uniform calibration.

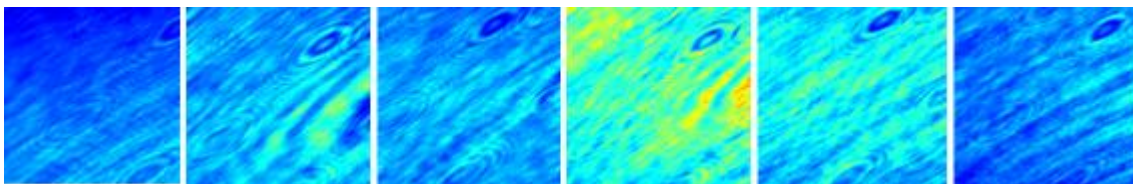


Figure 4.7: elements m_{00} of the Mueller matrix for the six wavelengths measured.

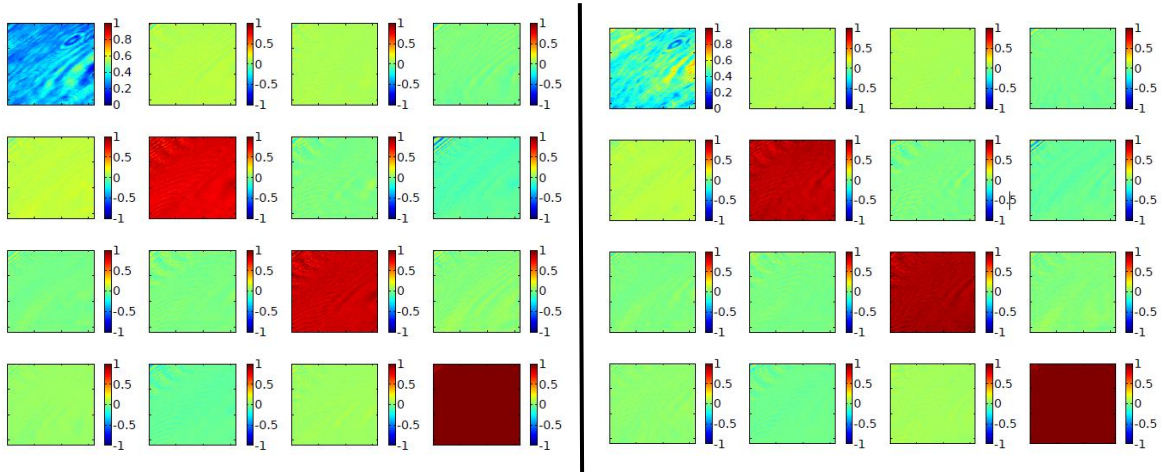


Figure 4.8: calibration Mueller matrices at wavelengths $\lambda_2 = 616 \text{ nm}$ and $\lambda_4 = 556 \text{ nm}$.

After doing these calibrations, we have studied some optical elements. We have done and spectral study of the behavior of a linear polarizer.

4.3.1. Study of a linear polarizer

The Muller matrices of an ideal linear polarizer at 0° , 90° and $\pm 45^\circ$ are:

$$\mathbf{M}_0 = \begin{bmatrix} 1 & 1 & 0 & 0 \\ 1 & 1 & 0 & 0 \\ 0 & 0 & 0 & 0 \\ 0 & 0 & 0 & 0 \end{bmatrix} \quad \mathbf{M}_{90} = \begin{bmatrix} 1 & -1 & 0 & 0 \\ -1 & 1 & 0 & 0 \\ 0 & 0 & 0 & 0 \\ 0 & 0 & 0 & 0 \end{bmatrix} \quad \mathbf{M}_{\pm 45} = \begin{bmatrix} 1 & 0 & \pm 1 & 0 \\ 0 & 0 & 0 & 0 \\ \pm 1 & 0 & 1 & 0 \\ 0 & 0 & 0 & 0 \end{bmatrix} \quad (4.3)$$

In general, the Mueller matrix of a linear polarizer with its transmission axis in an angle α would be [8]:

$$\mathbf{M}_\alpha = \begin{bmatrix} 1 & c_{2\alpha} & s_{2\alpha} & 0 \\ c_{2\alpha} & c_{2\alpha}^2 & s_{2\alpha}c_{2\alpha} & 0 \\ s_{2\alpha} & s_{2\alpha}c_{2\alpha} & s_{2\alpha}^2 & 0 \\ 0 & 0 & 0 & 0 \end{bmatrix} \quad (4.4)$$

Where $c_{2\alpha} = \cos(2\alpha)$ and $s_{2\alpha} = \sin(2\alpha)$.

We have measured the Mueller matrix of a low-quality linear polarizer, a dichroic-absorbing sheet, with its transmission axis at 90° (vertical) for the same wavelengths as the calibrations. Figure 4.9 shows the Mueller matrices of the polarizer at $\lambda_2 = 616 \text{ nm}$ and $\lambda_4 = 556 \text{ nm}$.

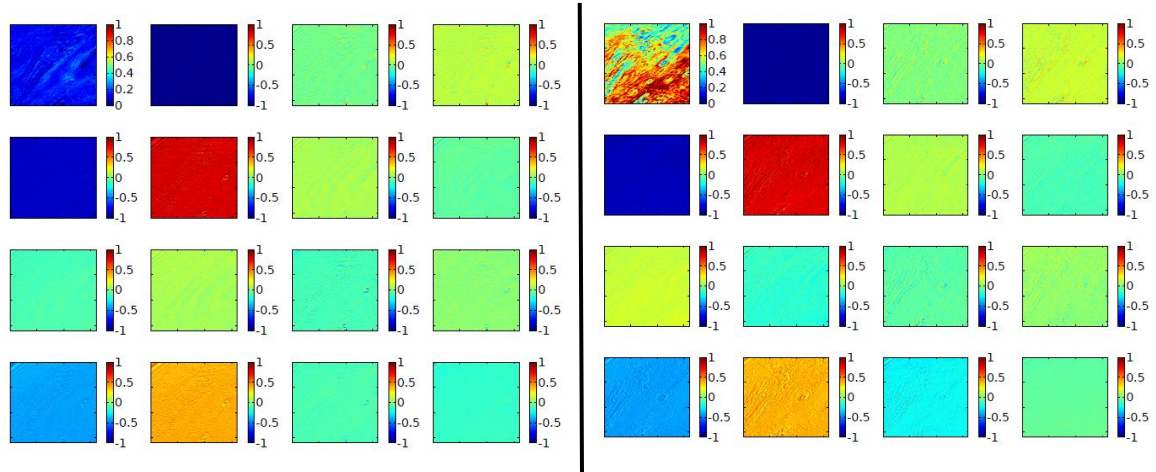


Figure 4.9: polarizer (transmission axis at 90° , vertical) Mueller matrices at wavelengths $\lambda_2 = 616 \text{ nm}$ and $\lambda_4 = 556 \text{ nm}$.

As we can see, this element behaves homogeneously in the observed area. The results of the MM at both wavelengths are pretty similar except for the inhomogeneities of the m_{00} element and the deviation from zero of some elements like m_{30} and m_{31} . These two elements are related to the phase of the output Stokes vector. In other words, this polarizer has a residual behavior as “retarder”.

For instance, making a rough analysis, if we approximate $m_{30} \approx -0.3$, this polarizer will introduce a phase of approximately $|\varphi| \approx \pi/20$ over a depolarized light beam ($\mathbf{S} = [1 \ 0 \ 0 \ 0]^T$).

Another change between the two matrices is in the elements m_{20} and m_{21} . These elements seem to be different from zero and to change the sign. This would be related to optical activity.

Therefore, at the exit of the polarizer we wouldn't have a perfectly linearly polarized beam, but the polarization would be an ellipse slightly rotated.

5. CONCLUSIONS AND FINAL REMARKS

The main goal of this project has been to improve the Dual Rotating Compensator Polarimeter (DRPC) placed at the Optics laboratory by replacing a He-Ne laser by a supercontinuum laser source. This laser provides a wide spectrum that can be used to perform measures of the Mueller Matrix at any desired wavelengths in the visible region.

In order to do that, several tasks have been carried out:

- Study of the basic theory about polarimetry: applications, Jones and Stokes Muller formalism, polarimeters...
- Handling the DRCP in the laboratory. This step implies learning how it works and how to perform a measure of the Mueller Matrix.
- The next step was learning how to operate the different parts of what it was going to be the source and monochromator: supercontinuum laser, rotating stage, diffraction grating...
- Then, all the elements were assembled and the monochromator was built, replacing the previous source (He-Ne laser) by the new setup.
- Once all the elements were in the correct place, the monochromator was characterized by means of an auxiliary setup shown in figure 3.3. We have measured the wavelength selected by the diaphragm as a function of the position of the stage (figure 4.5) and we have studied the spectral width of the transmitted light as a function of the diaphragm aperture (figure 4.4).
- After the characterization the whole set up was correctly aligned with the rest of the DRPC so that the light follows the appropriate path reaching the sample and the detector.
- Finally, the correct working of the whole set up was checked by obtaining some calibrations Mueller matrix at different wavelengths (figure 4.8).
- Also, we have done a spectral study of a linear polarizer. We have measured its Mueller matrix with its transmission axis at 90° at different wavelengths (figure 4.9).

Regarding future work, and concerning the proper working of the spectropolarimeter, it would be important trying to achieve a more homogeneous and constant intensity of the beam in order to obtain a better calibration matrix. (As we can see in figure 4.7, the intensity distribution in elements m_{00} is quite inhomogeneous. The same happens in the Mueller matrices of the polarizer).

Of course, now that we are able to perform measures at any desired wavelength in the visible region, it would be very interesting to study samples or system whose Mueller matrices may present a variation along the visible spectrum.

Ideally, a living tissue containing some kind of immersed inhomogeneity would reveal the capabilities of this system to identify and locate the embedded object. In practical terms, other dense media with some wavelength-selective embedded object could be devised, so that a systematic study could be accomplished.

6. BIBLIOGRAPHY

- [1] Michael F. Sterzik, Stefano Bagnulo² & Enric Pallé. “*Biosignatures as revealed by spectropolarimetry of Earthshine*”. *Nature*, Vol. 483, 64-66, March 2012.
- [2] H. Canovas, S.V. Jeffers, M. De Juan Ovelar, M. Rodenhuis & C.U. Keller. “In search of biosignatures.” *Nature*, Vol. 483, 64-66, March 2012.
- [3] James Hough. “*Polarimetry: a powerful diagnostic tool in astronomy*”. *A&G*, Vol. 47, June 2006.
- [4] J. Scott Tyo, Dennis L. Goldstein. “*Review of passive imaging polarimetry for remote sensing applications*”. *Applied Optics*, Vol. 45, N^o 22, August 2006.
- [5] Triple enlace. Polarimetría (II): Aplicaciones en Química.
<http://triplenlace.com/2012/11/25/polarimetria-ii-aplicaciones-en-quimica/>
- [6] Nirmalya Ghosh and I. Alex Vitkin. “*Tissue polarimetry: concepts, challenges, applications, and outlook*”. *Journal of Biomedical Optics*, Vol. 16(11), November 2011.
- [7] Andreas H. Hielscher, Angelia A. Eick. “*Diffuse backscattering Mueller matrices of highly scattering media*”. *Optics Express*, Vol. 1, N^o 13.
- [8] Juan Marcos Sanz Casado. “*Polarimetría de sistemas difusores con microestructuras: efectos de difusión múltiple*”. Julio 2010.
- [9] J. M. Sanz,* C. Extremiana, and J. M. Saiz. “*Comprehensive polarimetric analysis of Spectralon white reflectance standard in a wide visible range*”. *Applied Optics*. Vol. 52, N^o 24, August 2013.
- [10] Francesco Carmagnola, J.M Sanz and J.M Saiz. “*Development of a Mueller matrix imaging system for detecting objects embedded in turbid media*”
- [11] Craig F. Bohren. “*Absorption and Scattering light by small particles. Chapter 2: electromagnetic theory*”. John Wiley & Sons, 1998.
- [12] J.J. Gil. “*Polarimetric characterization of light and media*”. *Eur. Phys. J. Appl. Phys.* 40, 1–47 (2007).
- [13] Toralf Scharf. “*Polarized Liquid Crystals and Polymers*”. Chapter 1: polarized light. John Wiley & Sons, 2007

- [14] Russell A. Chipman. *Handbook of Optics. Chapter 22: Polarimetry*. McGraw Hill, 2009.
- [15] Shih-Yau Lu and Russell A. Chipman. *Interpretation of Mueller matrices based on polar decomposition.* J. Opt. Soc. Am. A/Vol. 13, No. 5/May 1996
- [16] R. R. Alfano* and S. L. Shapiro. *Observation of Self-Phase Modulation and Small-Scale filaments in crystal and glasses*. Physical Review Letters, Vol. 24, N° 11, March 1970.
- [17] Govind P. Agrawal. *Nonlinear fiber optics*. San Diego: Academic Press, 2001.
- [18] Christopher Palmer and Erwin Loewen. *Diffraction grating handbook. Chapter 2: the physics of diffraction gratings*. Newport Corporation, 2005
- [19] Diffraction grating GR13-1850 (Grating specifications). Thorlabs.
<http://www.thorlabs.com/thorcat/11700/GR13-1850-SpecSheet.pdf>
- [20] R.M.A. Azzam. *Photopolarimetric measurement of the Mueller matrix by Fourier analysis of a single detected signal*. Optical Letters, Vol. 2, N° 6. June 1978.
- [21] Femto Power 1060 Super Continuum Laser Source User's manual.
- [22] Rüdiger Paschotta. RP Photonic Encyclopedia (Mode Locking)
http://www.rp-photonics.com/mode_locking.html.
- [23] CR1-Z7, CR1/M-Z7 Motorized Rotation Stage Operating Manual. Thorlabs
<http://www.thorlabs.com/thorcat/17000/CR1-Z7-Manual.pdf>
- [24] TDC001 DC Servo Motor Driver User's Guide. Thorlabs.
- [25] USB2000 Fiber Optic Spectrometer Operating Instructions. Ocean Optics.

BLOCK II**1. INTRODUCTION**

Last year I was awarded a scholarship under the agreement between the University of Cantabria and the University of Brown (Providence, RI, USA).

From June 16th to August 8th, I stayed in the School of Engineering under the supervision of Prof. R. Zia [1].

This group works mainly in the fields of nanophotonics, materials science, optical physics, and physical chemistry. Specifically, they study the multipolar transitions and how light is emitted from solid-state quantum emitters (like atoms, defect centers, ions, molecules, and quantum dots).

They investigate new ways to control and enhance the process of light emission for photonic devices by developing new techniques to directly quantify and access specific transitions.

This research group receives students from the fields of physics and engineering. It is currently formed by four Ph.D. students and several undergrad students; all of them coordinated by Prof. Rashid Zia, the head of the group.

During my stay there, I have participated in the daily life and routines of the group, I attended several training courses and I have been assigned different tasks like preparing and attending oral presentations, helping other students at the lab or learning some specific concepts.

2. TASKS

2.1 *Daily life*

The first task I was assigned was to prepare an oral presentation, in order to show the rest of the group my work done back in Spain.

In the same way, during the weeks, I attended presentations prepared by the rest of the undergrad students, where they explained the work they were carrying out during the summer.

This included topics such as optical activity and chiral molecules, molecular scale imaging techniques or thermodynamics.

On the other hand, I attended the presentation of the PhD work of one of the students, a research about wide-angle energy-momentum spectroscopy [2].

This technique allows the simultaneous measurement of the momentum and spectral distribution of light emission and can reveal a lot of information about the electronic structure of the emitter.

He studies the emission rates for magnetic and electric dipole transitions in europium-doped yttrium oxide ($\text{Eu}^{3+}:\text{Y}_2\text{O}_3$) and chromium-doped magnesium oxide ($\text{Cr}^{3+}:\text{MgO}$). In order to do that, he images the back focal plane of a microscope objective to obtain the radiation pattern and project it onto two orthogonal polarizations with a Wollaston prism. Finally, he disperses them in the different wavelengths using a diffraction grating.

At the same time, some afternoons, undergrad student went down to the laboratory and help Ph.D. students and the Professor so that we could learn how to work in the lab.

For instance, I helped to assemble and align a setup for doing micro-photoluminescence-excitation-spectroscopy on very low concentration quantum emitters. The setup consisted of a white light source, several parabolic mirrors to guide and focus the light, a diffraction grating to expand the continuous spectrum, a slit to select a wavelength interval, a sample holder and a spectrometer. This experimental setup was specially interesting for its proximity with that of my UC project.

2.2. *Compulsory training courses*

In order to be allowed to work in the lab, it was necessary to attend several training courses. These courses were mandatory for all students, research staff, or

any person working in the different laboratories at Brown and they covered the basic knowledge and skills you have to acquire in order to work safely.

In my particular case, I attended three courses which included both classroom and online classes:

- Laser Safety Training:

It was an online course oriented to revise the main parts of a laser and the basic concepts and physics behind its working.

Also, it presented the classification of lasers regarding their power and its potential hazard (classes 1, 1M, 2, 2M, 3R, 3B and 4 from safer to more hazardous).

Of course, the course also explained the potential damages laser can make to eyes or skin depending on the wavelength, as well as, the security measures you have to take in order to safely work with the different classes of lasers.

- Hazardous Waste Training:

This course explained how the University of Brown manages (storage, pick-up routines and transport) wastes, specially hazardous wastes, generated at the labs.

I learnt to identify solid wastes and the regulations that show how they must be labeled and stored in a proper container depending on its characteristics, as well as how to proceed in case of an emergency involving hazardous wastes.

- Laboratory Safety Training:

This course covered different topics regarding the general safety in laboratories: emergency procedures, fire safety, electrical safety, an introduction to Chemical Hygiene Plan, Material Safety Data Sheets (MSDS), how to work with chemicals, security measures working on the lab (gloves, glasses, lab coat...), how to manage compressed gas cylinders, reactive chemical, fume hoods...

2.3. Movement of a rotating stage using Matlab Executable (Mex) files

Another task was to develop some programs written in C++ code in order to control the movement of a rotating stage using Mex-files.

We wanted the stage to perform two main movements: a home movement (return the stage to the origin) and an absolute movement (rotate the stage a certain angle).

In order to communicate with the stage we will use the Host-Controller Communications Protocol given by Thorlabs [3] and the D2XX functions [4]. The stage used is a PRM1Z8 Motorized Rotation Stage controlled by a TDC001 T-Cube DC Servo Motor Controller, both made by Thorlabs [5].

Mex-files [6], [7] are able to call C or Fortran routine directly from Matlab. Mex stands for Matlab Executable. This means that you can run a code written in C++ from Matlab as if it were a built-in function. Mex-files can be called exactly like M-functions in MATLAB.

In order to write a Mex-file we need to include a gateway routine: *mexFunctions*. Matlab uses it as the entry point to the function.

We need to write the following code:

```
#include "mex.h"

void mexFunction (int nlhs, mxArray *plhs[], int nrhs, const mxArray *prhs[]) {

    /* Here we write our C code ... For instance:*/

    mexPrintf("Hello World!");

}
```

Where *nlhs* is the number of output arguments, *nrhs* is the number of input arguments and *plhs* and *prhs* are arrays with the output and input arguments respectively.

Inside this gateway routine we can write our function in C code. The header *#include "mex.h"* is always necessary.

We save our program with the extension *hello.cpp*. The name of the file with the gateway will be the command name in Matlab. After this, we need to choose a suitable compiler (write `mex -setup` in the command window and select the compiler) and compile it by writing `mex hello.cpp`. Once the code is compiled we can call the file from the command window in Matlab as if it were a m-file.

For instance, when we type *hello* in the command window, the code above will print the words *Hello World!*

Using the commands described in reference [4] and [5] we were able to successfully compile the code and to initiate the communications with the stage. I explained how to use Mex-files to my teammate and he will continue working on this project.

3. BIBLIOGRAPHY

- [1] The Zia Lab. <http://www.zia-lab.com>
- [2] Christopher M. Dodson,* Jonathan A. Kurvits,* Dongfang Li, and Rashid Zia. School of Engineering and Department of Physics, Brown University, Providence, RI. "*Wide-angle energy-momentum spectroscopy.*"
- [3] Thorlabs APT Controllers Host-Controller Communications Protocol. http://www.sal.wisc.edu/manga/archive/public/datasheets/thorlabs/APT_Communications_Protocol_Rev%203.pdf
- [4] Software Application Development D2XX Programmer's Guide. [http://www.ftdichip.com/Support/Documents/ProgramGuides/D2XX_Programmer's_Guide\(FT_000071\).pdf](http://www.ftdichip.com/Support/Documents/ProgramGuides/D2XX_Programmer's_Guide(FT_000071).pdf)
- [5] PRM1Z8 Motorized Rotation Stage user's manual. <http://www.thorlabs.com/thorcat/19700/PRM1Z8-Manual.pdf>
- [6] Maria Axelsson. "*An introduction to MATLAB An introduction to MATLAB MEX Files.*" http://pages.cs.wisc.edu/~ferris/cs733/Seminarium_CBA_ht07_MATLAB_MEX_handouts.pdf
- [7] <http://www.mathworks.es/>

